Optical Coherence Tomography Optic Nerve Head Morphology in Myopia I: Implications of Anterior Scleral Canal Opening Versus Bruch Membrane Opening Offset

JIN WOOK JEOUNG, HONGLI YANG, STUART GARDINER, YA XING WANG, SEUNGWOO HONG, BRAD FORTUNE, MICHAËL J.A. GIRARD, CHRISTY HARDIN, PING WEI, MARCELO NICOLELA, JAYME R. VIANNA, BALWANTRAY C. CHAUHAN, AND CLAUDE F. BURGOYNE

• PURPOSE: To measure the magnitude and direction of anterior scleral canal opening (ASCO) offset relative to the Bruch membrane opening (BMO) (ASCO/BMO offset) to characterize neural canal obliqueness and minimum cross-sectional area (NCMCA) in 69 highly myopic and 138 healthy, age-matched, control eyes.

• DESIGN: Cross-sectional study.

• METHODS: Using optical coherence tomography (OCT) scans of the optic nerve head (ONH), BMO and ASCO were manually segmented and their centroids and size and shape were calculated. ASCO/BMO offset magnitude and direction were measured after projecting the ASCO/BMO centroid vector onto the BMO plane. Neural canal axis obliqueness was defined as the angle between the ASCO/BMO centroid vector and the vector perpendicular to the BMO plane. NCMCA was defined by projecting BMO and ASCO points onto a plane perpendicular to the neural canal axis and measuring their overlapping area.

• RESULTS: ASCO/BMO offset magnitude was greater (highly myopic eyes 264.3 ± 131.1 μm; healthy control subjects 89.0 ± 55.8 μm, $P < .001$, t test) and ASCO centroid was most frequently nasal relative to BMO centroid (94.2% of eyes) in the highly myopic eyes. BMO and ASCO areas were significantly larger ($P < .001$, t test), NCMCA was significantly smaller ($P < .001$), and all 3 were significantly more elliptical ($P \leq .001$) in myopic eyes. Neural canal obliqueness was greater in myopic (65.17° ± 14.03°) compared with control eyes (40.91° ± 16.22°; $P < .001$, t test).

• CONCLUSIONS: Our data suggest that increased temporal displacement of BMO relative to the ASCO, increased BMO and ASCO area, decreased NCMCA, and increased neural canal obliqueness are characteristic components of ONH morphology in highly myopic eyes. (Am J Ophthalmol 2020;218:105–119. © 2020 Elsevier Inc. All rights reserved.)

AJO.com Supplemental Material available at AJO.com.

Accepted for publication May 12, 2020.

From the Devers Eye Institute Optic Nerve Head Research Laboratory (J.W.J., H.Y., Y.X.W., C.H., P.W., C.F.B.) and the Devers Eye Institute Discoveries in Sight Research Laboratories (J.W.J., H.Y., S.G., Y.X.W., B.F., C.H., P.W., C.F.B.), Legacy Research Institute, Portland, Oregon, USA; Department of Ophthalmology (J.W.J.), Seoul National University Hospital, Seoul National University College of Medicine, Medical College, Catholic University of Korea, Seoul, Korea; and the Beijing Institute of Ophthalmology (Y.X.W.), Beijing Tongren Eye Center, Beijing Tongren Hospital, Beijing, China; Department of Ophthalmology and Visual Sciences (S.H.), Medical College, Catholic University of Korea, Seoul, Korea; Ophthalmic Engineering and Innovation Laboratory (M.J.A.G.), Department of Biomedical Engineering, National University of Singapore, Singapore; and the Department of Ophthalmology and Visual Sciences (M.N., J.R.V., B.C.C.), Dalhousie University, Halifax, Nova Scotia, Canada.

Drs Jeoung and Yang served jointly as first authors.

Presented in part at the Association for Research in Vision and Ophthalmology Annual Meeting, April 28-May 2, 2019, Vancouver, British Columbia, Canada.

Inquiries to Claude F. Burgoyne, Optic Nerve Head Research Laboratory, Legacy Devers Eye Institute, 1225 NE 2nd Ave, Portland, OR 97208-3950, USA; e-mail: cfburgoyne@deverseye.org

IN PATIENTS WITH AXIAL MYOPIA,[1] ELONGATION OF THE eye is accompanied by structural changes to the choroid, sclera, retina, and optic nerve head (ONH) tissues that contribute to the clinical appearance of tilt, torsion, and peripapillary atrophy of the myopic optic disc.[2–9] Recent optical coherence tomography (OCT) studies have described myopic alterations to the macular and peripapillary retina,[10–12] macular and peripapillary choroid,[13–15] lamina cribrosa,[16,17] and the Bruch membrane opening (BMO),[18] including longitudinal temporal BMO displacement.[19–21]

While refractive error is used to define myopia and axial length is commonly used to assess its progression,[1] at present there is no OCT parameterization strategy to quantify and stage the morphologic character of myopic alteration to the ONH neural and connective tissues. By "morphologic character" of myopic alteration we mean its magnitude, tissue composition, and sectoral extent. As such, there are also no OCT strategies to account for the presence of nonglaucomatous, myopic structural alteration to the ONH tissues when attempting to detect glaucomatous ONH alterations in highly myopic eyes.

In a recent study of 362 healthy human eyes,[22] we defined the term "neural canal" to be the connective tissue pathway of the retinal ganglion cell (RGC) axons

0002-9394/$36.00
https://doi.org/10.1016/j.ajo.2020.05.015

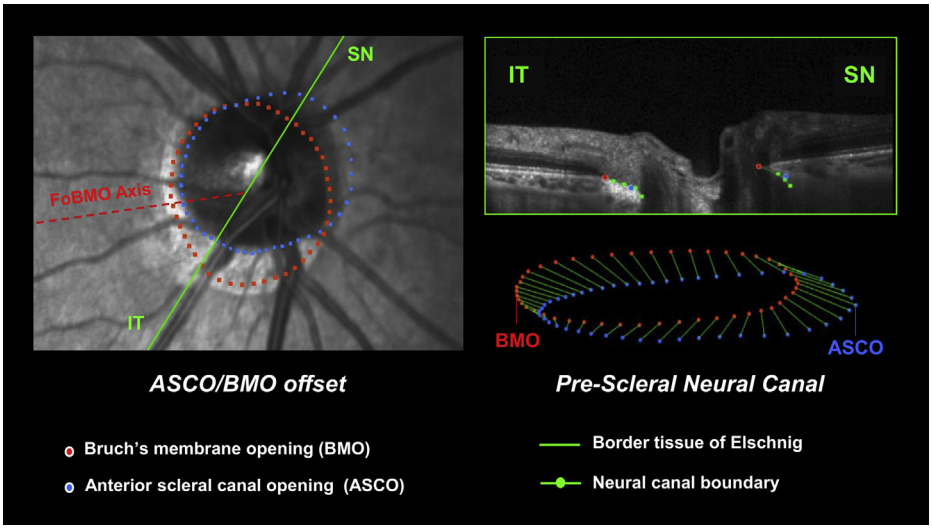

FIGURE 1. Optical coherence tomography (OCT) optic nerve head anatomic landmarks in a non–highly myopic healthy eye. (Left) Manually segmented Bruch membrane opening (BMO) and anterior scleral canal opening (ASCO) points from 24-radial OCT B-scans are shown relative to the fovea to BMO centroid (FoBMO) axis (red dotted line). Note that the BMO is inferior-temporally displaced relative to the deeper ASCO. The single green line shows the fundus location of the representative B-scan shown in the upper right panel. (Upper right) The neural canal landmark points segmented within a single OCT B-scan image (inferior-temporal [IT] left and superior-nasal [SN] right). In each radial B-scan, the ASCO was manually segmented on each side of the neural canal by visually projecting the plane of the juxtacanalicular anterior scleral surface through the neural canal boundary and marking their intersection (see Methods). (Lower right) The prescleral neural canal is defined by the position of the ASCO relative to the BMO. The 48 BMO and ASCO points along with the neural canal boundary points (the border tissues of Elshnig). All data are reported in right eye orientation. See Figure 2 for our definition for ASCO/BMO offset. Note also that this eye shows the classic pattern of internally oblique border tissues of Elschnig superior-nasally and externally oblique border tissues inferior temporally that directly follows from the position of the ASCO relative to the BMO in this eye.

through the ONH as they exit the eye to achieve the orbital optic nerve. We further defined it to extend from BMO through the anterior and posterior scleral canal openings and to consist of "prescleral" and "scleral canal" regions. We proposed that the size, shape and offset of the anterior scleral canal opening (ASCO) relative to BMO (ie, the ASCO/BMO offset) contributes to the direction, obliqueness, and minimum cross-sectional area (NCMCA) of the prescleral neural canal. We further predicted that incorporation of 3-dimensional neural canal connective tissue anatomy into OCT-based ONH phenotyping algorithms would eventually allow the magnitude of myopic ONH neural and connective tissue alteration in a given eye to be quantified separate from traditional measures of axial length or refractive error.

Our working hypothesis is that progressive temporal displacement of BMO relative to the ASCO (ie, progressive nasal ASCO/BMO offset),[19–23] BMO and ASCO enlargement and posterior bowing of the peripapillary sclera[24,25] are core components of ONH morphology that can be used to quantify and stage the morphologic character (ie, phenotype) of myopic alteration within a given ONH in future clinical and genetic studies. As a first step toward characterizing ONH neural canal connective tissue architecture in high myopia,[1] the purpose of the present study was to quantify the size, shape, and offset of the ASCO relative to BMO in highly myopic and non–highly myopic healthy eyes to determine ONH neural canal direction, obliqueness, and minimum cross-sectional area. Second, we wanted to determine the influence of ocular and demographic factors on these parameters.

Detecting and quantifying the clinical phenomenon of "temporal BMO displacement" in myopia is an important goal of this study. It is therefore also important to clarify that the parameter we developed for this purpose (ASCO/BMO offset, Figures 1 and 2) uses BMO as the reference opening and measures the offset of ASCO relative to BMO. This means that the clinical phenomenon of "temporal BMO offset" is detected and quantified as "nasal ASCO/BMO offset" within the conventions for that parameter. We choose this convention for defining ASCO/BMO offset because the RGC axons pass through BMO before reaching the ASCO within the neural canal and we felt our concepts of neural canal direction, neural canal obliqueness, and NCMCA were more clinically intuitive when the position of ASCO was characterized relative to BMO in this manner.

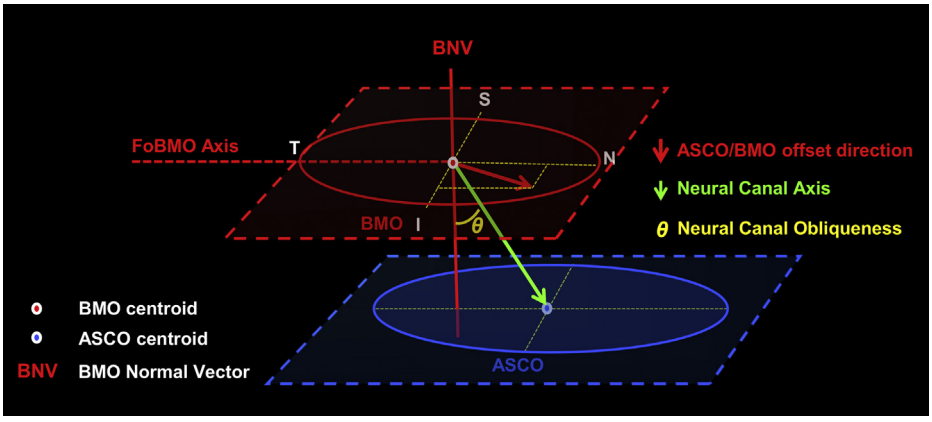

FIGURE 2. Anterior scleral canal opening (ASCO) offset relative to the Bruch membrane opening (BMO), the neural canal axis, and its direction and obliqueness. ASCO/BMO offset is defined by the vector connecting the BMO and ASCO centroids (the ASCO/BMO centroid vector here labeled (and also defined as) the neural canal axis after it has been projected to the BMO reference plane. ASCO/BMO offset magnitude is the length of the projected vector within the BMO reference plane. ASCO/BMO offset direction is calculated within the BMO reference plane relative to the fovea-BMO (FoBMO) axis (0° temporal, 90° superior, 180° nasal, and 270° inferior). The prescleral neural canal is defined by the position of the ASCO relative to the BMO. The prescleral neural canal axis (hereafter referred to as the neural canal axis), is also defined by the ASCO/BMO centroid vector, which is shown as a green arrow. Neural canal direction and ASCO/BMO offset direction are therefore identical, and within this article is primarily referred to as the ASCO/BMO offset direction. Neural canal obliqueness is defined by the angle of the neural canal axis relative to the BMO reference plane normal vector (BMO normal vector [BNV]; 0° directly perpendicular and 90° parallel to the plane of the BMO).

METHODS

• **STUDY SUBJECTS AND EYES:** Our study adhered to the Declaration of Helsinki for research involving human participants and was approved by the institutional review board of each participating institution. All participants provided written informed consent. Candidate eyes included 74 highly myopic eyes (inclusion criteria below) with and without glaucomatous visual field loss (GLVFL)[26,27] from 74 subjects and 362 eyes from 362 healthy subjects from a mixed ethnicity normative database.[22,25,28,29]

Subjects with highly myopic eyes with GLVFL were recruited prospectively from the glaucoma clinic at the Eye Care Centre, Queen Elizabeth II Health Sciences Centre, Halifax, Nova Scotia, Canada. Highly myopic eyes without GLVFL were recruited consecutively from attendees of a local optometry practice.[26,27] Highly myopic eye inclusion criteria included best-corrected visual acuity ≥20/40, spherical equivalent ≤ −6 diopters (D), or axial length ≥26.5 mm; astigmatism <4 D; absence of degenerative myopic changes in the macula; and absence of other retinal or optic nerve disease other than glaucoma.

Criteria for the diagnosis of "myopia with GLVFL" and "myopia without GLVFL" were described previously.[30] In brief, the diagnosis was assigned by consensus among 3 glaucoma subspecialists who evaluated the visual fields and optic disc photographs from all participants independently and were masked from all other demographic and clinical information. To minimize bias in defining glaucoma, visual field appearance was primarily used for designating the diagnostic group of the participants. Eyes were included in the myopic without GLVFL group if their visual field was graded as normal or with abnormalities consistent with myopia, but not glaucoma, independently by all 3 clinicians, irrespective of the grading given to their optic disc. If all 3 clinicians graded the visual field as having glaucomatous abnormalities, the eye was included in the myopic with GLVFL group. In cases in which the 3 clinicians disagreed on the visual field grading, the clinicians used their optic disc evaluation to achieve a consensus assignment into either the myopia with GLVFL or myopia without GLVFL cohorts.

Initially, 131 myopic eyes of 131 subjects were recruited for the study. All clinicians independently agreed that 42 eyes were glaucomatous and 72 eyes were nonglaucomatous based on visual field assessment (ie, complete agreement in 114 [87%] subjects). Of the remaining 17 (13%) eyes, consensus classification after the optic disc evaluation was reached in 16 eyes, whereas the remaining eye in which consensus was not obtained was excluded from the study.[27] Of these 131 myopic eyes, 74 highly myopic eyes (ie, with a myopic refractive error of > −6 D or an axial length ≥26.5 mm) were included for this study. In the present study, 5 eyes were excluded because of the poor quality of OCT images, leaving a final sample of 69 highly myopic study eyes (38 eyes without GLVFL and 31 eyes with GLVFL).

Because we reported significant age effects on several neural canal parameters in our previous study,[22] 138 age-

matched healthy control eyes for the 69 highly myopic study eyes were generated from the candidate group of 362 healthy eyes using a 1:2 case-control matching approach. Each matched set consisted of 1 highly myopic eye (case, n = 1) and 2 healthy control eyes (n = 2). The healthy control eyes were matched for age ± 5 years. This procedure was performed by 1 observer (J.W.J.) who was masked to the test results.

Inclusion criteria for the candidate group of 362 healthy eyes included: subject age 18-90 years; no history of glaucoma, intraocular pressure (IOP) ≤21 mm Hg; best-corrected visual acuity ≥20/40, refraction < ±6 D sphere and ±2 D cylinder, and glaucoma hemifield test and mean deviation within normal limits. Exclusion criteria included: unusable stereo photographs or insufficient OCT image quality (scan quality score <20); clinically abnormal optic disc appearance; any intraocular surgery (except uncomplicated cataract surgery); and any vitreous, retinal, choroidal, or neuro-ophthalmologic disease.

• **OCT IMAGE ACQUISITION, MAGNIFICATION ESTIMATION, AND SEGMENTATION:** For each eye, before OCT image acquisition the following measurements were made: visual acuity, refractive correction, curvature of the central, anterior corneal surface (by keratometry), axial length, and IOP (by Goldman applanation) were measured. OCT imaging was then performed, and the eyes were dilated, if necessary, for fundus photographic acquisition. ONH, peripapillary retinal nerve fiber layer (pRNFL), and macula were imaged with spectral-domain OCT (Spectralis, Heidelberg Engineering GmbH, Heidelberg, Germany, software version Heyex 1.9.10.0). To image each eye, the operator manually identified and marked the fovea in a live B-scan, then centered the imaging field on the ONH, where the 2 BMO points in each of 2 perpendicular ONH radial B-scans were identified.[31] These steps established the eye-specific, fovea-BMO (FoBMO) axis, which was used as the reference for the acquisition of all subsequent OCT B-scans.[30] The complete ONH imaging pattern consisted of 24 radial B-scans (15° apart with each B-scan containing 768 A-scans) centered on BMO. Each radial B-scan was acquired 25 times (in enhanced depth imaging[32] mode), and averaged in real time to enhance its signal to noise ratio.

Magnification correction in the healthy control eyes was achieved by the proprietary Spectralis operating software, which uses keratometry measurements (entered into the acquisition module before imaging) and a refractive error estimate derived from the focus setting of the camera head when the operator has brought the retinal image into focus (Heidelberg Engineering Spectralis user manual). That system software is based on the Gullstrand schematic eye model and assumes a default axial length of 24.385 mm. In the highly myopic eyes, the OCT acquisition protocol of the previous study[27] used a default value of 7.7 mm rather than the eye-specific keratometry value. Therefore, in order to account for potential effects of lateral magnification error, a post hoc adjustment of lateral pixel size was determined for each highly myopic eye using the eye-specific keratometry value and a Gullstrand schematic eye model[33] similar to that incorporated within the Spectralis OCT system software (as confirmed previously by personal communication between Brad Fortune and Gerhard Zinser of Heidelberg Engineering, April 2009).

Our methods of OCT image manual segmentation have been described in detail previously.[22,28,29,31] In brief, raw OCT volumes were exported from the device and imported into a custom 3-dimensional visualization and segmentation software (Devers Eye Institute, ATL 3D Suite, Portland, Oregon, USA).[34] ONH and peripapillary landmarks were manually segmented in each radial B-scan and the ONH was reconstructed 3-dimensionally (Figure 1). Segmented landmarks included: the internal limiting membrane (ILM); the posterior surface of the pRNFL, the posterior surface of the Bruch membrane/retinal pigment epithelium complex, BMO, neural canal wall, anterior scleral surface, and the ASCO (segmented on each side of the canal by visually projecting the plane of the peripapillary anterior scleral surface through the neural canal wall and marking their intersection).[28,29] All manual segmentations were performed by 2 observers (P.W., C.H.) within the Optic Nerve Head Research Laboratory of Devers Eye Institute. Quantification of all parameters was performed within custom software (Matlab version 7.3.0.267; The MathWorks, Natick, Massachusetts, USA). All left eye data were converted to right eye configuration for analysis.

• **FOVEA-BMO AND FOVEA-ASCO DISTANCE:** Fovea-BMO Distance was measured within the confocal scanning laser ophthalmoscopy (CSSO) image plane as the distance between the BMO centroid and center of the macula lutea. Fovea-ASCO distance was measured as the distance between the ASCO centroid and the center of the fovea projection in micrometers. Both parameters thus measure a 2-dimensional projection of the distance (ie, a chord) between these 2 landmarks rather than the actual distance along the curved surface of the retina.

• **ONH NEURAL CANAL CONNECTIVE TISSUE PARAMETERS:** Detailed descriptions of the following parameters, along with an illustrative video, are published elsewhere.[22] All data are reported in right eye orientation.

BMO and ASCO size and shape. A plane was fitted to the 48 segmented BMO and ASCO points, respectively (Figure 2), satisfying a least mean square error restraint in each case.[35] Then, the BMO points were projected to the best-fit BMO plane. Using the projected points, a best-fit ellipse was determined[35] and the BMO centroid, area, and ovality index (ellipse long axis length/ellipse short axis length) were calculated. An ASCO centroid, area, and shape index were similarly calculated within the ASCO plane.

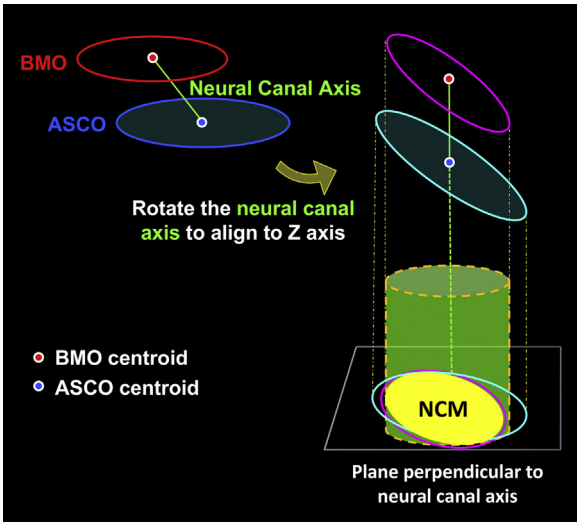

FIGURE 3. Neural canal minimum cross-sectional area (NCMCA). The NCMCA is calculated within a plane that is perpendicular to the neural canal axis (the neural canal perpendicular plane). The NCMCA estimates the smallest opening through which the retinal ganglion cell axons pass as they leave the eye. It is calculated by generating a neural canal perpendicular plane, projecting the Bruch membrane opening (BMO) and anterior scleral canal opening (ASCO) points onto it and quantifying the area that is common to both projections (yellow area).

ASCO/BMO offset magnitude and direction. ASCO/BMO offset magnitude and direction were defined by projecting the ASCO/BMO centroid vector (connecting the BMO and ASCO centroids) to the BMO plane (Figure 2). ASCO/BMO offset magnitude was defined within the BMO plane as the length of the ASCO/BMO vector component within the BMO plane. ASCO/BMO offset direction was defined within the BMO reference plane by the angle between the projected ASCO/BMO centroid vector and the FoBMO axis (0˚) measured clockwise relative to the FoBMO axis (superior 90˚, nasal 180˚, and inferior 270˚).

Neural canal axis, direction and obliqueness. The neural canal axis was defined by the ASCO/BMO centroid vector as described above (Figure 2). Neural canal direction and ASCO/BMO offset direction are therefore identical, were measured identically, and are most commonly referred to as ASCO/BMO offset direction within this manuscript. Neural canal obliqueness was defined by the angle between the neural canal axis vector and a vector perpendicular to the BMO plane, originating at the BMO centroid (Figure 2).

NCMCA. NCMCA (Figure 3) estimates the smallest opening through which the RGC axons pass as they leave the eye. It is calculated within a plane that is perpendicular to the neural canal axis (the neural canal perpendicular plane), by projecting the BMO and ASCO points onto it and quantifying the area that is common to both projections (Figure 3). NCMCA ovality index was calculated as outlined for BMO and ASCO (NCMCA ovality index = ellipse long axis length/ellipse short axis length).

• **MANUAL SEGMENTATION REPRODUCIBILITY:** The reproducibility of our study parameters within the 362 healthy, non–highly myopic human eyes from which the healthy control eyes were chosen, has been previously reported to be excellent.[22] Because of the known difficulty in segmenting BMO in highly myopic eyes,[36] we assessed interdelineator reproducibility within the highly myopic eyes of this report by having 2 delineators independently segment 6 of the highly myopic eyes that were chosen to span the range of axial length present within the 68 highly myopic eyes of this study.

• **STATISTICAL ANALYSIS:** Descriptive statistics included the mean and standard deviation for continuous variables and the proportions for categorical variables. Interobserver reproducibility was assessed with the intraclass correlation coefficient of each variable. Baseline characteristics and all OCT ONH parameters were compared between the 2 groups with the *t* test for continuous variables and χ^2 test for categorical variables.

For multiple comparisons, the Holm-Bonferroni method[37] was used to adjust for type I error. Factors associated with all neural canal connective tissue parameters were initially evaluated with univariable linear regression analysis. Factors associated with each dependent variable with a $P \leq .10$ were evaluated in multivariable regression models. Before the multivariable analysis, collinearity between the independent variables was evaluated with correlation analysis. All statistical analyses were performed with IBM SPSS Statistics (v 24.0, IBM Corp, Armonk, New York USA) and GraphPad Prism (v 8.1.2, GraphPad Software, Inc, San Diego, California, USA). $P < .05$ was considered statistically significant.

RESULTS

• **SUBJECT CHARACTERISTICS:** The demographic and ocular characteristics of the 69 highly myopic study subjects and 138 age-matched control subjects are summarized in Table 1. By design, there was no significant difference in the mean age between highly myopic (57.3 ± 9.2) and healthy control subjects (57.2 ± 9.4). As expected, the refraction, axial length, fovea-BMO centroid distance, global pRNFL thickness, and

TABLE 1. Demographic and Ocular Characteristics of the Study Participants and Eyes

	Highly Myopic Eyes, n = 69 Mean (SD)	Healthy Control Eyes, n = 138 Mean (SD)	*P* Value
Age, y (SD)	57.3 (9.2)	57.2 (9.4)	.927
Female gender, n (%)	33 (47.8)	81 (58.7)	.138
Left eye, n (%)	34 (49.3)	61 (44.2)	.490
IOP on imaging day, mm Hg (SD)	15.4 (3.5)	14.6 (2.8)	.070
CCT, μm (SD)	550.7 (37.2)	558.1 (29.8)	.126
Refraction, diopters (SD)	−7.61 (2.27)	-0.14 (1.82)	<.001[a]
Axial length, mm (SD)	26.96 (1.07)	23.62 (0.96)	<.001[a]
Cornea curvature, mm (SD)	7.76 (0.32)	7.71 (0.25)	.2752
Fovea-BMO distance, μm (SD)	4458.8 (473.3)	4391.0 (282.8)	<.001[a]
Fovea-ASCO distance μm (SD)	4672.4 (524.8)	4444.0 (298.6)	<.001[a]
Global pRNFLT, μm (SD)	74.2 (13.9)	96.4 (10.5)	<.001[a]
Global MRW, μm (SD)	231.2 (81.1)	328.0 (58.9)	<.001[a]

ASCO = anterior scleral canal opening; BMO = Bruch's membrane opening; CCT = central corneal thickness; IOP = intraocular pressure; MRW = minimum rim width; pRNFLT = peripapillary retinal nerve fiber layer thickness (measured at fixed 12 degree diameter); SD = standard deviation.

[a]Statistically significant differences ($P < .05$, *t* test or χ^2 test) that remain significant using a correction for multiple comparisons (Holm-Bonferroni method).

TABLE 2. Bruch's Membrane Opening, Anterior Scleral Canal Opening, and Neural Canal Characteristics of Highly Myopic Versus Age-Matched Control Eyes

	Highly Myopic Eyes, n = 69 (Mean ± SD)	Healthy Control Eyes, n = 138 (Mean ± SD)	*P* Value
BMO area (mm^2)	2.323 ± 0.798	1.795 ± 0.354	<.001[a]
ASCO area (mm^2)	2.263 ± 0.750	2.166 ± 0.402	<.001[a]
NCMCA (mm^2)	0.857 ± 0.559	1.280 ± 0.378	<.001[a]
BMO ovality index	1.132 ± 0.086	1.125 ± 0.058	<.001[a]
ASCO ovality index	1.145 ± 0.087	1.127 ± 0.063	<.001[a]
NCMCA ovality index	2.780 ± 0.979	1.557 ± 0.567	<.001[a]
ASCO/BMO offset magnitude (μm)	264.3 ± 131.1	89.0 ± 55.8	<.001[a]
ASCO/BMO offset direction (degrees)	156.4 ± 37.5	140.6 ± 61.5	<.001[a]
Neural canal obliqueness (degrees)	65.17 ± 14.03	40.91 ± 16.22	<.001[a]

ASCO = anterior scleral canal opening; BMO = Bruch's membrane opening; NCMCA = neural canal minimum cross-sectional area; ovality index = ellipse long axis/ellipse short axis; SD = standard deviation.

[a]Statistically significant differences ($P < .05$, *t* test) that remain significant using a correction for multiple comparisons (Holm-Bonferroni method).

global minimum rim width (MRW) were significantly different between highly myopic and healthy control eyes ($P < .001$, *t* test).

While comparisons between highly myopic eyes with (n = 38) and without (n = 31) GLVFL were not a primary goal of this study, there were significant differences in age, IOP on examination day, axial length, global pRNFL thickness, global MRW, and visual field mean deviation between the 2 subgroups ($P < .05$, *t* test). However, only axial length, global pRNFL thickness, global MRW, and mean deviation remained significant after applying a Holm-Bonferroni correction for multiple comparisons (Supplemental Table 1).

• **INTEROBSERVER REPRODUCIBILITY:** Study parameter intraclass correlation coefficient values for the highly myopic eyes of this study were excellent, ranging from 0.836-0.998.

• **HIGHLY MYOPIC VERSUS HEALTHY CONTROL EYE COMPARISONS:** *Fovea-BMO and fovea-ASCO distance*. Both the fovea-BMO distance (4458.8 μm [473.3] vs 4391.0 μm [282.8]) and the fovea-ASCO distance (4672.4 μm [524.8] vs 4444.0 μm [298.6]; $P < .001$, *t* test corrected for multiple comparisons, Table 1) were increased in the highly myopic compared to the healthy control eyes.

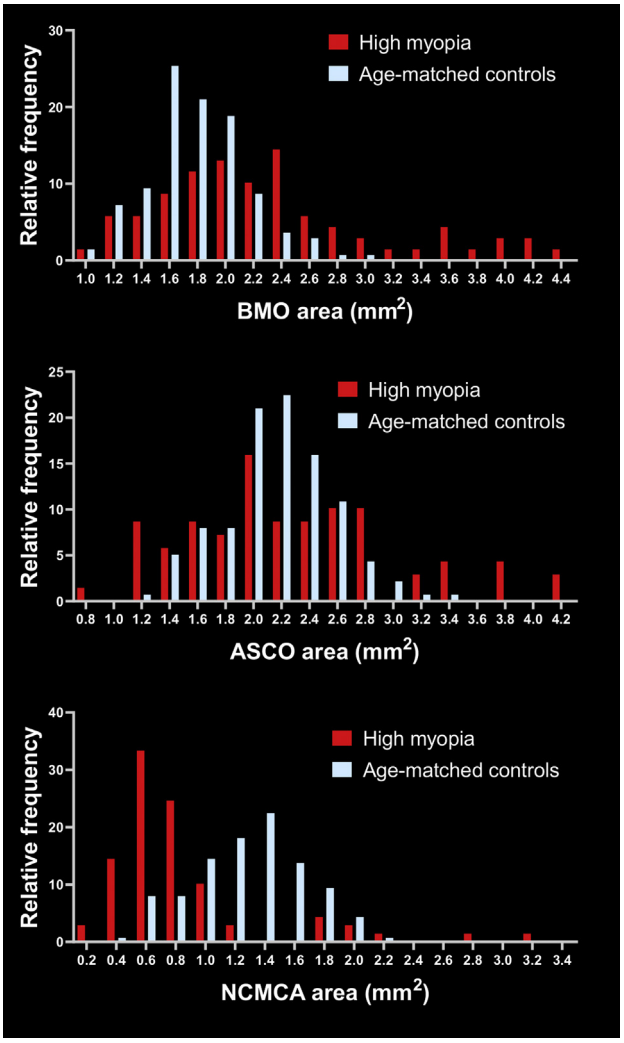

FIGURE 4. Distribution and frequency of the Bruch's membrane opening (BMO) area (upper), anterior scleral canal opening (ASCO) area (middle) and neural canal minimum cross-sectional area (NCMCA) (lower) among highly myopic vs age-matched healthy control eyes.

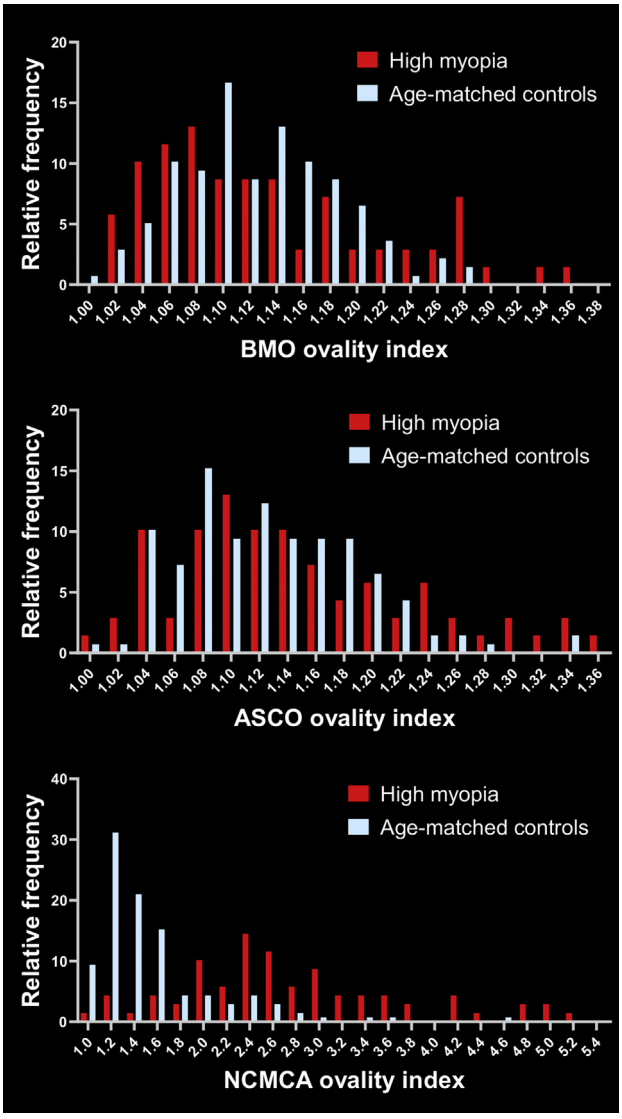

FIGURE 5. Distribution and frequency of Bruch's membrane opening (BMO) ovality, anterior scleral canal opening (ASCO) ovality (middle), and neural canal minimum cross-sectional area (NCMCA) ovality (lower) among highly myopic vs age-matched healthy control eyes.

BMO, ASCO, and NCMCA size and shape. The BMO and ASCO areas of highly myopic eyes (2.323 ± 0.798 mm^2 and 2.263 ± 0.750 mm^2) were significantly larger than those of the healthy control eyes (1.795 ± 0.354 mm^2 and 2.166 ± 0.402 mm^2, respectively; $P < .001$, t test). NCMCA was significantly smaller in the highly myopic eyes (0.857 ± 0.559 mm^2) compared with control eyes (1.280 ± 0.378 mm^2; $P < .001$, t test). BMO, ASCO, and NCMCA ovality indices were significantly higher in highly myopic eyes compared with control eyes ($Ps \leq .001$, t test). These differences remained significant after correction for multiple comparisons (Table 2, Figures 4 and 5).

ASCO/BMO offset magnitude and direction. ASCO/BMO offset magnitude was significantly larger in myopic eyes (264.3 ± 131.1 μm) compared with control eyes (89.0 ± 55.8 μm; $P < .001$, t test). The angle of ASCO/BMO offset direction was significantly larger in myopic eyes (156.4° ± 37.5° relative to the FoBMO axis) compared with control eyes (140.6° ± 61.5°; $P < .001$, t test). These parameters remained significant after correction for multiple comparisons (Table 2).

ASCO/BMO offset within the highly myopic and healthy control eyes is depicted in Figure 6. ASCO/BMO offset direction was nasal in 65 of the 69 highly myopic

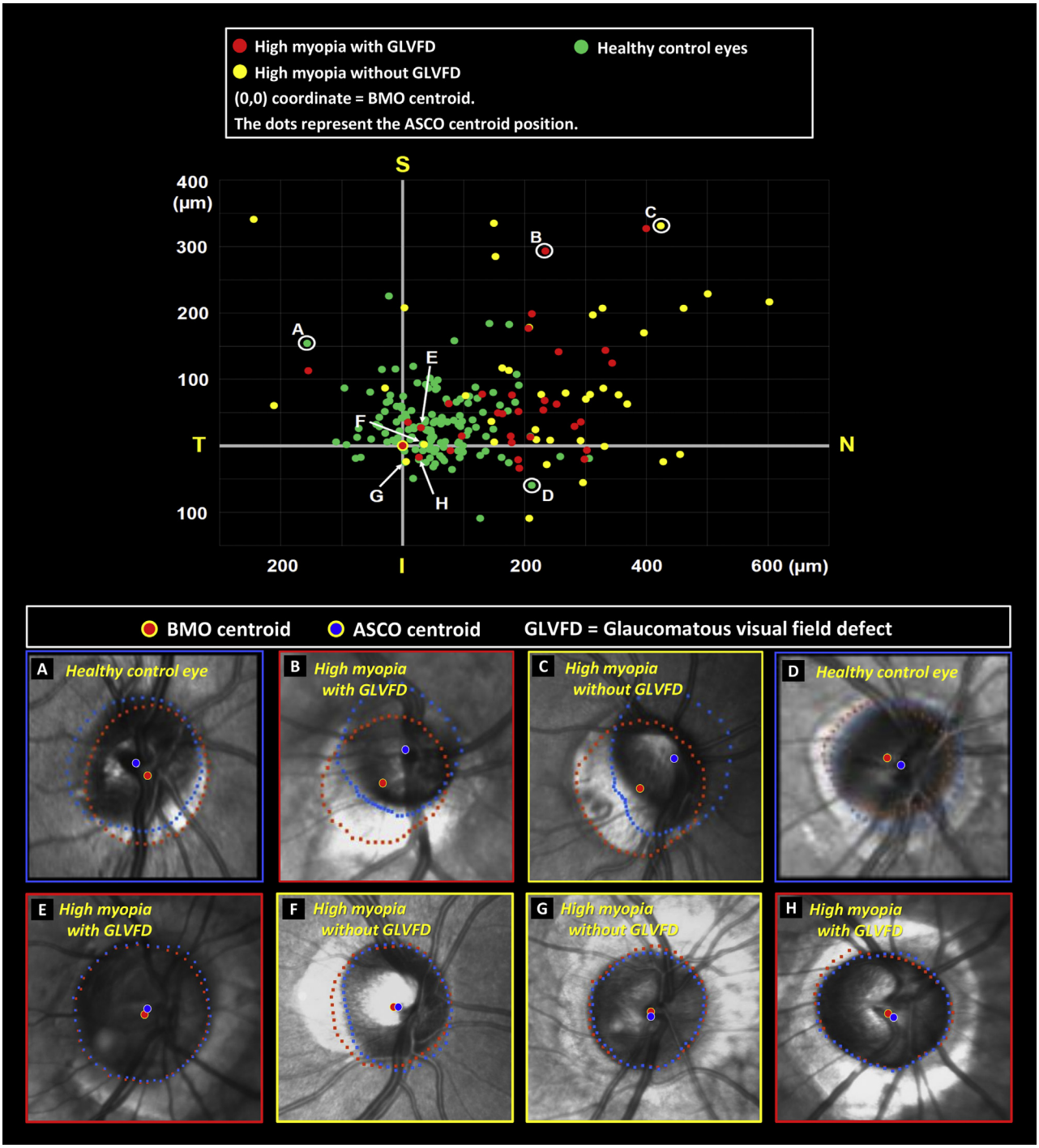

FIGURE 6. Distribution of anterior scleral canal opening (ASCO) vs Bruch's membrane opening (BMO) offset among highly myopic vs age-matched healthy control eyes (upper panel) with representative cases (lower panel). Two-dimensional plot of the position of the ASCO centroid relative to the BMO centroid for all study eyes. The BMO centroid of each eye is located at the origin (0, 0) coordinate. By convention, ASCO/BMO offset direction is 0° when it is directly temporal (T), 90° when superior (S), 180° when nasal (N), and 270° when inferior (I). (Bottom panel, upper row) Representative eyes from the extreme locations. (Bottom panel, lower row) Representative eyes with "low" magnitude of ASCO/BMO offset (red dots, BMO points; central red dot with white border, BMO centroid; blue dots, ASCO points; central blue dot with white border, ASCO centroid; blue outline, healthy control eye; red outline, high myopia with glaucomatous visual field defect [GLVFD]; yellow outline, high myopia without GLVFD). All data are in right eye orientation. Note that given the conventions of our ASCO/BMO offset parameter, the clinical phenomenon of temporal displacement of BMO relative to the ASCO is detected as "nasal ASCO/BMO offset."

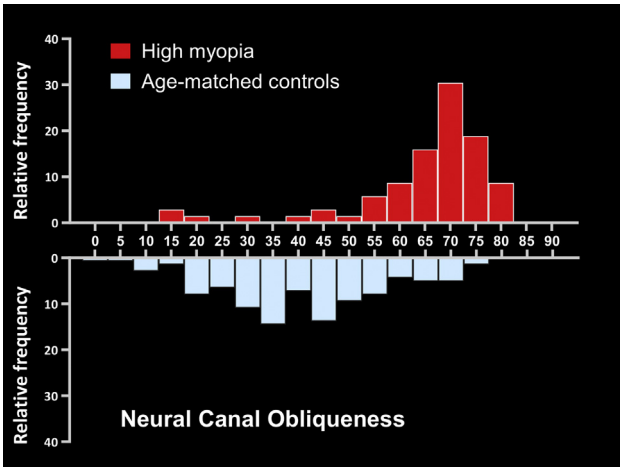

FIGURE 7. Distribution and frequency of neural canal obliqueness among highly myopic vs age-matched healthy control eyes.

eyes (94.2%). Superior-nasal offset was more frequent in highly myopic (75.4%) compared with healthy control eyes (60.2%; $P = .017$, χ^2 test). The clinical appearance of representative highly myopic and healthy control eyes demonstrating a range of ASCO/BMO offset magnitude and direction are also shown in Figure 6.

Neural canal obliqueness. The distribution and frequency of neural canal obliqueness in the highly myopic and healthy control eyes are depicted in Figure 7. Mean neural canal obliqueness was significantly greater in the highly myopic ($65.17^\circ \pm 14.03^\circ$) compared with healthy control eyes ($40.91^\circ \pm 16.22^\circ$; $P < .001$, t test with Holm-Bonferroni criterion adjustment, Table 2). In Figure 8 neural canal obliqueness is superimposed on the ASCO/BMO offset data from Figure 6, indicating that the eyes demonstrating the greatest ASCO/BMO offset also demonstrate the greatest obliqueness.

• **OCULAR AND DEMOGRAPHIC FACTORS ASSOCIATED WITH ASCO/BMO OFFSET AND NCMCA:** We used linear regression analyses to identify factors associated with ASCO/BMO offset and NCMCA. Axial length ($\beta = 24.137$; 95% confidence interval 15.145-33.130; $P < .001$) was associated with ASCO/BMO offset in healthy control eyes within multivariable analysis (Table 3). In multivariable analysis, axial length (highly myopic eyes: $\beta = 0.157$, $P = .012$; healthy control eyes: $\beta = -0.143$; $P < .001$) was associated with NCMCA (Table 4). Axial length was significantly correlated to NCMCA ($R^2 = 0.106$, $P = .007$) within the highly myopic eyes (Table 5).

• **NEURAL CANAL CONNECTIVE TISSUE CHARACTERISTICS OF HIGHLY MYOPIC EYES WITH AND WITHOUT GLVFL:** Our assessment of statistically significant neural canal connective tissue parameter differences between the 2 highly myopic eye subsets are reported in Table 6. While ASCO/BMO offset magnitude was significantly larger in the highly myopic without glaucomatous field loss eyes compared with highly myopic with glaucomatous field loss eyes ($P = .009$, t-test), this difference did not remain significant after applying a Holm-Bonferroni correction for multiple comparisons.

DISCUSSION

OCT CHARACTERIZATION OF THE OCULAR TISSUES IN HIGHly myopic eyes has been limited to measurements of MRW,[31] pRNFLT,[12,38,39] laminar depth,[18] curvature,[40] thickness,[41] peripapillary choroidal thickness,[13–15,29] and macular retinal ganglion cell layer and pRNFLT thickness.[11,42] However, Hasegawa and associates[23] recently used OCT imaging to report nasal displacement of the anterior scleral canal opening relative to BMO in a group of 101 glaucoma and glaucoma suspect eyes that included highly myopic eyes. In that study, measurements were limited to the nasal and temporal regions of the ONH only. Similar to the present study, they reported that the magnitude of nasal displacement of the scleral canal opening relative to BMO correlated with axial length.

Our study expands upon the findings of the Hasegawa report by using a 3-dimensional parameterization strategy and by comparing highly myopic to age-matched non–highly myopic eyes. In so doing it lays a foundation for expanding OCT phenotyping of myopic eyes in future clinical and genetic studies to include quantification of ASCO/BMO offset, neural canal direction and obliqueness, NCMCA, as well as recently published measurements of peripapillary sclera bowing.[24,25] Through comparison with non–highly myopic normative databases,[22,28,29,31,43,44] the ultimate goal of this work is to account for the magnitude of myopic structural alterations within a given highly myopic eye so as to improve the diagnostic precision of glaucoma detection. To be able to address glaucoma detection in the future, we included highly myopic eyes with glaucoma in the highly myopic group of study eyes to ensure that our methods could also capture their ONH morphology.

The principal findings of this study are as follows. First, while BMO and ASCO areas were significantly larger, NCMCA was significantly smaller in highly myopic compared with healthy control eyes. Second, BMO, ASCO, and NCMCA were significantly more elliptical in myopic compared with healthy control eyes. Third, ASCO/BMO offset magnitude was greater and its direction was more commonly superior nasal in highly myopic compared with healthy control eyes. Fourth, neural canal obliqueness was significantly greater in myopic compared with healthy control eyes. Fifth, fovea-BMO and fovea-ASCO distances were both greater in highly myopic

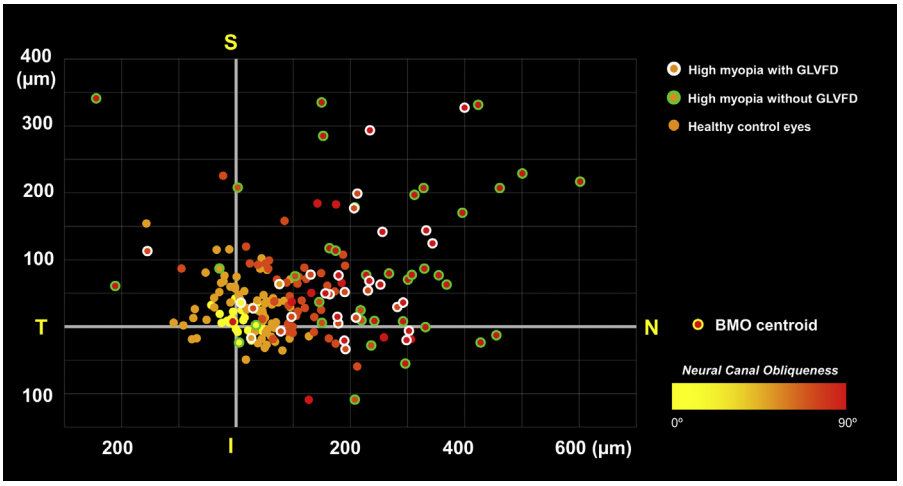

FIGURE 8. Color map of anterior scleral canal opening (ASCO) vs Bruch's membrane opening (BMO) offset relative to neural canal obliqueness among highly myopic vs age-matched healthy control eyes. Two-dimensional plot of the position of the ASCO centroid relative to the BMO centroid for all study eyes with color grading according to the degree of neural canal obliqueness (red colored dot, the greatest degree [90°] of neural canal obliqueness; yellow colored dot, the lowest degree [0°] of neural canal obliqueness). As expected, neural canal obliqueness is strongly correlated to ASCO/BMO offset being greatest (red colored dots) in the eyes that are most offset and least (yellow colored dots) in the eyes that are least offset (dot with white border, high myopia with glaucomatous visual field defect [GLVFD]; dot with green border, high myopia without GLVFD; dot without border, healthy control eye). All data are in right eye orientation. Note that given the conventions of our ASCO/BMO offset parameter, the clinical phenomenon of temporal displacement of BMO relative to the ASCO is detected as "nasal ASCO/BMO offset."

TABLE 3. Factors Associated With Anterior Scleral Canal Opening/Bruch's Membrane Opening Offset

	Univariable		Multivariable	
	β (95% CI)	*P* Value	β (95% CI)	*P* Value
Highly myopic eyes				
Age, per 1 year older	−0.029 (−3.506 to 3.449)	.987		
Female gender	−33.601 (−96.594 to 29.392)	.291		
CCT, per 1 μm larger	1.119 (0.306-1.933)	.008[a]	0.748 (−0.099 to 1.595)	.082
Axial length, per 1 mm larger	−32.480 (−61.345 to −3.615)	.028[a]	−19.562 (−48.593 to 9.470)	.183
IOP on imaging day, per 1 mm Hg higher	12.788 (4.170-21.406)	.004[a]	8.044 (−1.325 to 17.413)	.091
Healthy control eyes				
Age, per 1 year older	0.179 (−0.829 to 1.187)	.726		
Female gender	−10.073 (−29.146 to 9.001)	.298		
CCT, per 1 μm larger	0.014 (−0.304 to 0.332)	.930		
Axial length, per 1 mm larger	24.137 (15.145-33.130)	<.001[a]	24.137 (15.145-33.130)	<.001[a]
IOP on imaging day, per 1 mm Hg higher	−0.424 (−3.859 to 3.011)	.807		

CCT = central corneal thickness; CI = confidence interval; IOP = intraocular pressure.
[a]Statistically significant effects ($P < .05$, linear regression test).

compared with healthy control eyes. Finally, axial length was significantly correlated with ASCO/BMO offset magnitude and NCMCA in the highly myopic eyes.

While increased "optic disc size" in highly myopic eyes has been previously reported based on histologic estimates[45] and photographic assessment of the clinical disc margin,[46,47] few OCT studies have rigorously assessed BMO area in high myopia and no previous OCT studies have assessed ASCO area or NCMCA in highly myopic eyes. Using OCT imaging, Lee and associates[18] reported that BMO area correlated with axial length in both eyes of 10 "healthy" and 17 glaucomatous highly myopic subjects which corresponds well with our observations. An early study by Leung and associates[48] used confocal

TABLE 4. Factors Associated With the Neural Canal Minimum Cross-Sectional Area

	Univariable		Multivariable	
	β (95% CI)	*P* Value	β (95% CI)	*P* Value
Highly myopic eyes				
Age, per 1 year older	0.004 (−0.011 to 0.019)	.594		
Female gender	0.016 (−0.255 to 0.287)	.907		
CCT, per 1 μm larger	−0.003 (−0.007 to 0.000)	.060[a]	−0.003 (−0.006 to 0.001)	.140
Axial length, per 1 mm larger	0.173 (0.053 to 0.294)	.005[a]	0.157 (0.036-0.279)	.012[a]
IOP on imaging day, per 1 mmHg higher	−0.029 (−0.067 to 0.010)	.138		
Healthy control eyes				
Age, per 1 year older	−0.005 (−0.011 to 0.002)	.178		
Female gender	−0.027 (−0.157 to 0.102)	.678		
CCT, per 1 μm larger	0.001 (−0.002 to 0.003)	.558		
Axial length, per 1 mm larger	−0.143 (−0.206 to -−0.081)	<.001[a]	−0.143 (−0.206 to −0.081)	<.001[a]
IOP on imaging day, per 1 mmHg higher	0.002 (−0.021 to 0.026)	.846		

CCT = central corneal thickness; CI = confidence interval; IOP = intraocular pressure.
[a]Statistically significant effects ($P < .05$, linear regression test).

TABLE 5. Correlation Analysis Between Axial Length and Anterior Scleral Canal Opening/Bruch's Membrane Opening Offset Magnitude, Bruch's Membrane Opening Area, Anterior Scleral Canal Opening Area, and Neural Canal Minimum Cross-Sectional Area in Highly Myopic Eyes

	Axial Length vs ASCO/BMO Offset Magnitude	Axial Length Vs BMO Area	Axial Length vs ASCO Area	Axial Length vs NCMCA	Axial Length vs Fovea-BMO Distance	Axial Length vs Fovea-ASCO Distance
Pearson r[a]	–0.206	0.112	0.095	0.325	0.042	0.001
R^2	0.042	0.013	0.009	0.106	0.002	<0.0001
P value	.091	.364	.440	.007[b]	.7298	0.9911

ASCO = anterior scleral canal opening; BMO = Bruch membrane opening; CI = confidence interval; NCMCA = neural canal minimum cross-sectional area.
[a]Adjusted for mean deviation of visual field test.
[b]Statistically significant effect ($P < .05$, Pearson correlation test).

scanning tomography and time-domain OCT imaging to report an increase in the size of the optic disc with increasing axial length, though disc area was defined using HRT based on the clinical disc margin, and was undefined anatomically using OCT.

In our study eyes, NCMCA was significantly smaller in highly myopic compared with healthy control eyes. This finding likely follows from the fact that NCMCA is defined to be the area of overlap between the projections of BMO and ASCO onto a plane perpendicular to the neural canal axis, and this area of overlap decreases the more the ASCO is offset from BMO. The fact that ASCO/BMO offset increased and NCMCA decreased in proportion to axial length in the highly myopic eyes supports these relationships.

NCMCA may have clinical significance in highly myopic eyes as the size and shape of the NCMCA may influence the amount of neuronal tissue as well as its susceptibility within the ONH.[22] In non–highly myopic healthy eyes, we recently reported an R^2 value for the correlation between NCMCA and global pRNFLT (0.158) that was 4-fold higher than that between BMO area and pRNFLT (0.038), which is the current OCT standard for "correcting" the amount of neural retinal rim and pRNFL tissue in a given eye for the "size" of the neural canal.[31,43] pRNFLT has previously been shown to be negatively correlated to axial length in highly myopic eyes.[12] Future studies of large numbers of highly myopic eyes will be required to determine the clinical importance of NCMCA to predict the "expected" pRNFLT for a given highly myopic eye as well as its relative susceptibility to glaucomatous alteration.[22]

BMO, ASCO, and NCMCA were all more elliptical in the highly myopic compared with healthy control eyes. Our BMO findings correspond well with the results of a previous study[18] that reported that BMO was larger and more

TABLE 6. Bruch's Membrane Opening, Anterior Sclera Canal Opening, And Neural Canal Characteristics of the Highly Myopic Eyes With and Without Glaucomatous Visual Field Loss

	Highly Myopic Eyes (n = 69)		
	Highly Myopic Eyes Without GLVFL (n = 38)	Highly Myopic Eyes With GLVFL (n = 31)	*P* Value[a]
BMO area (mm^2)	2.378 ± 0.754	2.257 ± 0.856	.534
ASCO area (mm^2)	2.256 ± 0.691	2.271 ± 0.828	.938
NCMCA (mm^2)	0.792 ± 0.411	0.937 ± 0.700	.286
BMO ovality index	1.149 ± 0.092	1.111 ± 0.075	.073
ASCO ovality index	1.161 ± 0.090	1.126 ± 0.080	.091
NCMCA ovality index	2.960 ± 0.985	2.559 ± 0.941	.090
ASCO/BMO offset magnitude (μm)	301.0 ± 137.9	219.4 ± 108.1	.009[a]
ASCO/BMO offset direction (degrees)	154.8 ± 42.3	158.4 ± 31.3	.692
Neural canal obliqueness (degrees)	66.47 ± 13.84	63.58 ± 14.32	.398

ASCO = anterior sclera canal opening; BMO = Bruch's membrane opening; GLVFL = glaucomatous visual field loss; NCMCA = neural canal minimum cross-sectional area; SD = standard deviation.

[a]Statistically significant differences ($P < .05$, *t* test). None of these remained significant using a correction for multiple comparisons (Holm-Bonferroni method).

elliptical and that both correlated with axial length in highly myopic eyes.

The fact that both ASCO/BMO offset magnitude and neural canal obliqueness were greater in the highly myopic compared with healthy control eyes and that ASCO/BMO offset direction was more commonly superior nasal in the highly myopic eyes are important because they strongly support findings of four previous studies,[19–21,23] which collectively suggest that a temporal displacement of BMO relative to ASCO is a core component of myopic alteration to the ONH connective tissues. However, unlike these previous reports, which hypothesize primary nasal displacement of the ASCO and or contained lamina,[19–21] we emphasize that the longitudinal or cross-sectional detection of temporal displacement of BMO relative to the ASCO provides no insight as to which opening is stable and which opening is moving.

Until proven otherwise, we predict that as the sclera remodels in response to the signals that drive myopic elongation of the eye, both structures become displaced relative to one another with a net temporal displacement of BMO relative to the ASCO being the most common endpoint of this remodeling. We[29] and others[27] have previously outlined the effects of BMO temporal displacement relative to the ASCO on the border tissues of Elschnig and peripapillary choroidal thickness. The predictive power of characterizing this component of the myopic ONH on global RNFLT, on the sectoral distribution of pRNFLT, on peripapillary choroidal atrophy, and on long-term axonal survival remain to be determined.

Our findings that fovea-BMO centroid and fovea-ASCO centroid distances were greater in the highly myopic compared with healthy control eyes support the concepts outlined above but differ from the findings and interpretations of previous reports. Kim and associates[19] performed longitudinal OCT imaging in children with progressive myopia and reported no increase in the distance between the temporal border of BMO and the fovea. From this finding they concluded that the retina, temporal to BMO, did not expand in axial myopia during childhood. In that study, the ASCO was not segmented, no assessment of the position of BMO relative to the ASCO was made and BMO was segmented and measured in 3 horizontal B-scans instead of the 24 radial B-scans of the current report. Although the BMO diameter data derived from these scans clearly suggest a progressive increase in BMO diameter over 4 longitudinal visits, this increase did not achieve statistical significance and the authors concluded that BMO did not expand in childhood myopia. Jonas and associates[19,49] used similar techniques as Kim and associates[19] to report that the distance between the temporal border of BMO and the fovea was not increased in highly myopic eyes.

Pertinent to this discussion, it must be acknowledged that because our measurements are based on projections of the fovea and the ASCO or BMO centroids onto the CSLO image plane, they underestimate the actual continuous distance along the retinal surface between these landmarks, especially in eyes with substantial posterior (outward) peripapillary scleral bowing. While this might mean that the myopic vs control eye differences we report are underestimated, both projections are also subject to lateral magnification artifacts induced by axial elongation itself.[50,51] Additional longitudinal studies that include these measurements are necessary to clarify these issues.

We believe that the increased fovea-ASCO centroid distance in the highly myopic eyes of the current study is a manifestation of progressive expansion of the portion of the posterior sclera that contains the ASCO and underlies the fovea.[50,51] We hypothesize that the ASCO expands

and in most eyes becomes more oval as part of this posterior scleral expansion. We believe that the increased fovea-BMO centroid distance in the highly myopic eyes separately suggests that the Bruch's membrane and the retina also expand.[52] We also hypothesize that BMO enlarges and becomes more oval as a result of asymmetric Bruch's membrane expansion. Finally, we hypothesize that the net movement of the Bruch membrane relative to the sclera most commonly leaves BMO in a position that is temporal to the ASCO. This movement requires the border tissues of Elschnig (which physically connects BMO to ASCO) to remodel accordingly, and this remodeling underlies the classic pattern of border tissues being internally oblique nasally and externally oblique temporally, as we and others have described (see Figure 1 legend).[29,35]

Finally, while axial length was correlated with ASCO/BMO offset, neural canal obliqueness, and NCMCA in this study, the most extreme cases of ASCO/BMO offset, neural canal obliqueness, and NCMCA did not occur in the eyes with the greatest axial length, nor did all of the highly myopic eyes fall out of the range of the non–highly myopic eyes for any given parameter. These findings reflect the fact that the correlations with axial length were modest and suggest that the ONH alterations of axial myopia, while driven by the scleral alterations of axial elongation, likely will not be staged on the basis of axial length alone.

Our study is limited by the following considerations. First, while we studied a relatively small number of highly myopic eyes, we believe our data provide proof of concept that our parameters can be used to quantify the magnitude and character of myopic ONH connective tissue alteration in a given eye. Second, because we included myopic eyes with and without GLVFL, it can be imagined that a portion of our findings are related to glaucomatous ONH alterations that are independent from the alterations of axial myopia alone. There were significant differences in age, IOP on examination day (lower in eyes with GLVFL), axial length, global pRNFL thickness, global MRW, and visual field mean deviation between the 2 highly myopic subgroups ($P < .05$, t test). However, only axial length, global pRNFL thickness, global MRW, and mean deviation remained significant after applying a Holm-Bonferroni correction for multiple comparisons (Supplemental Table 1).

Finally, in a Spectralis OCT data set, the transverse dimensions of the pixel assigned to each A-scan is determined by a proprietary algorithm within the operating software that is based on the Gullstrand eye model (see Methods). While it is possible that the increases in ASCO/BMO offset, BMO area, ASCO area, FoBMO distance, and FoASCO distance with axial length we report are related to magnification correction error in highly myopic eyes, 2 findings argue against this being likely. First, we also report that NCMCA was substantially decreased in highly myopic eyes, which would not be expected if the error in magnification was consistent. Second, the associations between each of these parameters and axial length either do not achieve significance or the associations are weak.

Previous studies[53–56] have shown that glaucoma most commonly occurs at statistically normal levels of IOP in highly myopic eyes. While global MRW and pRNFLT measurements of the neuronal tissues were 30% and 23% smaller in the highly myopic with GLVFL eyes, respectively, none of our connective tissue parameters demonstrated significant differences between the 2 groups (after criterion adjustment to account for multiple comparisons). While the level of IOP at the time of imaging was modestly associated with ASCO/BMO offset only, the influence of IOP on these parameters may increase in larger studies that include eyes with higher levels of IOP. Finally, in any group of highly myopic eyes without glaucoma, there is potentially a subset of eyes undergoing early glaucomatous alteration (even at normal levels of IOP) under the threshold of clinical suspicion. We believe that this is likely true of the highly myopic eyes without GLVFL in this study.

In summary, we used OCT to quantify the size, shape, and offset of the ASCO relative to BMO so as to determine the direction, obliqueness, and minimum cross-sectional area of the ONH neural canal in highly myopic and healthy control eyes. Our cross-sectional data strongly suggest that increased temporal displacement of BMO relative to the ASCO (nasal ASCO/BMO offset), enlargement and increased ovality of BMO and ASCO, and reduction and increased ovality of NCMCA are core components of myopic alteration to the ONH tissues. Our data also suggest that the posterior sclera and posterior retina expand and shift relative to one another in axial myopia and we propose that this observation be confirmed in longitudinal studies. Finally, further studies with large numbers of highly myopic eyes with and without GLVFL are required to incorporate our neural canal parameters into strategies to separate the ONH structural alterations of glaucoma from the structural alterations of axial myopia in highly myopic eyes.

FUNDING/SUPPORT: SUPPORTED BY A NATIONAL EYE INSTITUTE GRANT (NIH/NEI R01-EY021281), A GRANT FROM THE CANADIAN National Institute for the Blind–Canadian Glaucoma Clinical Research Council; with supplemental support from a Mathers Fellowship award; Legacy Good Samaritan Foundation; and Heidelberg Engineering, GmbH, Heidelberg, Germany.

JW. Jeoung: None. H. Yang: None. S. Gardiner: Nonfinancial support–Heidelberg Engineering. YX. Wang: None. SW. Hong: None. B. Fortune: Financial support - Legacy Good Samaritan Foundation, Inotek Pharmaceuticals. M. Girard: Financial support - Abyss Processing Pte Ltd. C. Hardin: None. P. Wei: None. M. Nicolela: None. J. R. Vianna: None. B. C. Chauhan: Financial support - Heidelberg Engineering. C. F. Burgoyne: Financial support - NIH/NEI R01-EY021281, Legacy Good Samaritan Foundation, Heidelberg Engineering.

The above listed sponsors/funding organizations had no role in the design, conduct, analysis or reporting of this research.

Other Acknowledgments: All authors have completed and submitted the ICMJE form for disclosure of potential conflicts of interest. Financial Disclosures: All authors attest that they meet the current ICMJE criteria for authorship.

REFERENCES

1. Flitcroft DI, He M, Jonas JB, et al. IMI - defining and classifying myopia: a proposed set of standards for clinical and epidemiologic studies. *Invest Ophthalmol Vis Sci* 2019;60(3): M20–M30.
2. Hwang YH, Yoo C, Kim YY. Characteristics of peripapillary retinal nerve fiber layer thickness in eyes with myopic optic disc tilt and rotation. *J Glaucoma* 2012;21(6):394–400.
3. Hwang YH, Yoo C, Kim YY. Myopic optic disc tilt and the characteristics of peripapillary retinal nerve fiber layer thickness measured by spectral-domain optical coherence tomography. *J Glaucoma* 2012;21(4):260–265.
4. Park HY, Choi SI, Choi JA, Park CK. Disc torsion and vertical disc tilt are related to subfoveal scleral thickness in open-angle glaucoma patients with myopia. *Invest Ophthalmol Vis Sci* 2015;56(8):4927–4935.
5. Yamashita T, Sakamoto T, Yoshihara N, et al. Circumpapillary course of retinal pigment epithelium can be fit to sine wave and amplitude of sine wave is significantly correlated with ovality ratio of optic disc. *PLoS One* 2015;10(4): e0122191.
6. Suh SY, Le A, Shin A, Park J, Demer JL. Progressive deformation of the optic nerve head and peripapillary structures by graded horizontal duction. *Invest Ophthalmol Vis Sci* 2017; 58(12):5015–5021.
7. Yamashita T, Sakamoto T, Yoshihara N, et al. Correlations between local peripapillary choroidal thickness and axial length, optic disc tilt, and papillo-macular position in young healthy eyes. *PLoS One* 2017;12(10):e0186453.
8. Shoji T, Kuroda H, Suzuki M, Ibuki H, Araie M, Yoneya S. Vertical asymmetry of lamina cribrosa tilt angles using wide bandwidth, femtosecond mode-locked laser OCT; effect of myopia and glaucoma. *Graefes Arch Clin Exp Ophthalmol* 2017;255(1):197–205.
9. Shoji T, Kuroda H, Suzuki M, et al. Correlation between lamina cribrosa tilt angles, myopia and glaucoma using OCT with a wide bandwidth femtosecond mode-locked laser. *PLoS One* 2015;9(12):e116305.
10. Leung CK, Mohamed S, Leung KS, et al. Retinal nerve fiber layer measurements in myopia: an optical coherence tomography study. *Invest Ophthalmol Vis Sci* 2006;47(12): 5171–5176.
11. Choi YJ, Jeoung JW, Park KH, Kim DM. Glaucoma detection ability of ganglion cell-inner plexiform layer thickness by spectral-domain optical coherence tomography in high myopia. *Invest Ophthalmol Vis Sci* 2013;54(3):2296–2304.
12. Seo S, Lee CE, Jeong JH, Park KH, Kim DM, Jeoung JW. Ganglion cell-inner plexiform layer and retinal nerve fiber layer thickness according to myopia and optic disc area: a quantitative and three-dimensional analysis. *BMC Ophthalmol* 2017;17(1):22.
13. Flores-Moreno I, Lugo F, Duker JS, Ruiz-Moreno JM. The relationship between axial length and choroidal thickness in eyes with high myopia. *AmJ Ophthalmol* 2013;155(2): 314–319.e1.
14. Gupta P, Cheung CY, Saw S-M, et al. Peripapillary choroidal thickness in young Asians with high myopia. *Invest Ophthalmol Vis Sci* 2015;56(3):1475–1481.
15. Gupta P, Saw SM, Cheung CY, et al. Choroidal thickness and high myopia: a case-control study of young Chinese men in Singapore. *Acta Ophthalmol* 2015;93(7):e585–e592.
16. Jonas JB, Xu L. Histological changes of high axial myopia. *Eye (Lond)* 2014;28(2):113–117.
17. Jonas JB, Kutscher JN, Panda-Jonas S, Hayreh SS. Lamina cribrosa thickness correlated with posterior scleral thickness and axial length in monkeys. *Acta Ophthalmol* 2016;94(8): e693–e696.
18. Lee S, Han SX, Young M, Beg MF, Sarunic MV, Mackenzie PJ. Optic nerve head and peripapillary morphometrics in myopic glaucoma. *Invest Ophthalmol Vis Sci* 2014; 55(7):4378–4393.
19. Kim M, Choung HK, Lee KM, Oh S, Kim SH. Longitudinal changes of optic nerve head and peripapillary structure during childhood myopia progression on OCT: Boramae Myopia Cohort Study report 1. *Ophthalmology* 2018;125(8): 1215–1223.
20. Lee KM, Choung HK, Kim M, Oh S, Kim SH. Positional change of optic nerve head vasculature during axial elongation as evidence of lamina cribrosa shifting: Boramae Myopia Cohort Study report 2. *Ophthalmology* 2018;125(8): 1224–1233.
21. Kim TW, Kim M, Weinreb RN, Woo SJ, Park KH, Hwang JM. Optic disc change with incipient myopia of childhood. *Ophthalmology* 2012;119(1):21–26. e1–3.
22. Hong S, Yang H, Gardiner SK, et al. OCT-detected optic nerve head neural canal direction, obliqueness, and minimum cross-sectional area in healthy eyes. *Am J Ophthalmol* 2019; 208:185–205.
23. Hasegawa T, Akagi T, Hangai M, et al. Structural dissociation of optic disc margin components with optic disc tilting: a spectral domain optical coherence tomography study. *Graefes Arch Clin Exp Ophthalmol* 2016;254(2):343–349.
24. Tun TA, Wang X, Baskaran M, et al. Variation of peripapillary scleral shape with age. *Invest Ophthalmol Vis Sci* 2019; 60(10):3275–3282.
25. Wang YX, Yang H, Luo H, et al. Peripapillary scleral bowing increases with age and is inversely associated with peripapillary choroidal thickness in healthy eyes. *Am J Ophthalmol* 2020; https://doi.org/10.1016/j.ajo.2020.03.050.
26. Malik R, Belliveau AC, Sharpe GP, Shuba LM, Chauhan BC, Nicolela MT. Diagnostic accuracy of optical coherence tomography and scanning laser tomography for identifying glaucoma in myopic eyes. *Ophthalmology* 2016;123(6): 1181–1189.
27. Vianna JR, Malik R, Danthurebandara VM, et al. Beta and gamma peripapillary atrophy in myopic eyes with and without glaucoma. *Invest Ophthalmol Vis Sci* 2016; 57(7):3103–3111.
28. Luo H, Yang H, Gardiner SK, et al. Factors influencing central lamina cribrosa depth: a multicenter study. *Invest Ophthalmol Vis Sci* 2018;59(6):2357–2370.

29. Yang H, Luo H, Gardiner SK, et al. Factors influencing optical coherence tomography peripapillary choroidal thickness: a multicenter study. *Invest Ophthalmol Vis Sci* 2019;60(2):795–806.
30. Chauhan BC, Burgoyne CF. From clinical examination of the optic disc to clinical assessment of the optic nerve head: a paradigm change. *Am J Ophthalmol* 2013;156(2):218–227.e2.
31. Chauhan BC, Danthurebandara VM, Sharpe GP, et al. Bruch's membrane opening minimum rim width and retinal nerve fiber layer thickness in a normal white population: a multicenter study. *Ophthalmology* 2015;122(9):1786–1794.
32. Spaide RF, Koizumi H, Pozzoni MC. Enhanced depth imaging spectral-domain optical coherence tomography. *Am J Ophthalmol* 2008;146(4):496–500.
33. Atchison DA, Smith G. Schematic eyes. In: Atchison DA, Smith G, eds. Optics of the Human Eye. Oxford, UK: Butterworth-Heinemann; 2002.
34. Fortune B, Reynaud J, Hardin C, Wang L, Sigal IA, Burgoyne CF. Experimental glaucoma causes optic nerve head neural rim tissue compression: a potentially important mechanism of axon injury. *Invest Ophthalmol Vis Sci* 2016;57(10):4403–4411.
35. Strouthidis NG, Yang H, Fortune B, Downs JC, Burgoyne CF. Detection of optic nerve head neural canal opening within histomorphometric and spectral domain optical coherence tomography data sets. *Invest Ophthalmol Vis Sci* 2009;50(1):214–223.
36. Zheng F, Wu Z, Leung CKS. Detection of Bruch's membrane opening in healthy individuals and glaucoma patients with and without high myopia. *Ophthalmology* 2018;125(10):1537–1546.
37. Holm S. A simple sequentially rejective multiple test procedure. *Scand J Stat* 1979;6(2):65–70.
38. Biswas S, Lin C, Leung CK. Evaluation of a myopic normative database for analysis of retinal nerve fiber layer thickness. *JAMA Ophthalmol* 2016;134(9):1032–1039.
39. Seol BR, Kim DM, Park KH, Jeoung JW. Assessment of optical coherence tomography color probability codes in myopic glaucoma eyes after applying a myopic normative database. *Am J Ophthalmol* 2017;183:147–155.
40. Ha A, Kim TJ, Girard MJA, et al. Baseline lamina cribrosa curvature and subsequent visual field progression rate in primary open-angle glaucoma. *Ophthalmology* 2018;125(12):1898–1906.
41. Park HY, Jeon SH, Park CK. Enhanced depth imaging detects lamina cribrosa thickness differences in normal tension glaucoma and primary open-angle glaucoma. *Ophthalmology* 2012;119(1):10–20.
42. Lam DSC, Leung KS, Mohamed S, et al. Regional variations in the relationship between macular thickness measurements and myopia. *Invest Ophthalmol Vis Sci* 2007;48(1):376–382.
43. Araie M, Iwase A, Sugiyama K, et al. Determinants and characteristics of Bruch's membrane opening and Bruch's membrane opening-minimum rim width in a normal Japanese population. *Invest Ophthalmol Vis Sci* 2017;58(10):4106–4113.
44. Zangalli CS, Vianna JR, Reis ASC, et al. Bruch's membrane opening minimum rim width and retinal nerve fiber layer thickness in a Brazilian population of healthy subjects. *PLoS One* 2018;13(12):e0206887.
45. Jonas JB, Ohno-Matsui K, Panda-Jonas S. Optic nerve head histopathology in high axial myopia. *J Glaucoma* 2017;26(2):187–193.
46. Jonas JB, Gusek GC, Guggenmoos-Holzmann I, Naumann GO. Size of the optic nerve scleral canal and comparison with intravital determination of optic disc dimensions. *Graefes Arch Clin Exp Ophthalmol* 1988;226(3):213–215.
47. Oliveira C, Harizman N, Girkin CA, et al. Axial length and optic disc size in normal eyes. *Br J Ophthalmol* 2007;91(1):37–39.
48. Leung CK, Cheng AC, Chong KK, et al. Optic disc measurements in myopia with optical coherence tomography and confocal scanning laser ophthalmoscopy. *Invest Ophthalmol Vis Sci* 2007;48(7):3178–3183.
49. Jonas JB, Wang YX, Zhang Q, Liu Y, Xu L, Wei WB. Macular Bruch's membrane length and axial length. The Beijing Eye Study. *PLoS One* 2015;10(8):e0136833.
50. Norman RE, Flanagan JG, Rausch SM, et al. Dimensions of the human sclera: thickness measurement and regional changes with axial length. *Exp Eye Res* 2010;90(2):277–284.
51. Vurgese S, Panda-Jonas S, Jonas JB. Scleral thickness in human eyes. *PLoS One* 2012;7(1):e29692.
52. Choi SS, Enoch JM, Kono M. Evidence for transient forces/strains at the optic nerve head in myopia: repeated measurements of the Stiles–Crawford Effect of the First Kind (SCE-I) over time. *Ophthalmic Physiol Opt* 2004;24(3):194–206.
53. Mitchell P, Hourihan F, Sandbach J, Wang JJ. The relationship between glaucoma and myopia: the Blue Mountains Eye Study. *Ophthalmology* 1999;106(10):2010–2015.
54. Xu L, Wang Y, Wang S, Wang Y, Jonas JB. High myopia and glaucoma susceptibility the Beijing Eye Study. *Ophthalmology* 2007;114(2):216–220.
55. Grodum K, Heijl A, Bengtsson B. Refractive error and glaucoma. *Acta Ophthalmol Scand* 2001;79(6):560–566.
56. Kim MJ, Kim MJ, Kim HS, Jeoung JW, Park KH. Risk factors for open-angle glaucoma with normal baseline intraocular pressure in a young population: the Korea National Health and Nutrition Examination Survey. *Clin Experiment Ophthalmol* 2014;42(9):825–832.